Pair creation with bound electron for photon impact on bare heavy nuclei

Carsten K. Agger and Allan H. Sørensen

Institute of Physics and Astronomy, University of Aarhus, DK-8000 Aarhus C, Denmark

In this paper we present numerical calculations for the process of bound-free electron-positron pair production following photon impact on bare nuclei. The calculations are based on exact Coulomb waves. We include total as well as differential cross sections for production of both K and L electrons for a wide range of photon energies and nuclear charge numbers. Significant deviations from lowest-order Born theory appear for moderate and high charge numbers in both the total cross section and, most dramatically, in the angular distributions of the emitted positrons. Our results for total K-shell cross sections for photon impact as well as for ion impact, in the latter case as estimated by the virtual photon method, basically confirm those of Aste *et al.* [Phys. Rev. A **50**, 3980 (1994)]. However, we note that by inclusion of L-electron production, the cross section for the ion-induced process is increased by approximately 20% for heavy elements. [S1050-2947(97)05701-6]

I. INTRODUCTION

In recent years, a large effort has been devoted to the study of atomic physics processes in relativistic heavy-ion collisions [1]. In part, these investigations have been motivated by the practical importance of such processes. For instance, electron-positron pair creation with the electron produced directly in a bound state of one of the colliding bare ions, so-called bound-free pair production, is expected to become the dominant mechanism for beam loss and luminosity limitations in relativistic heavy-ion colliders [2].

Collisions involving ions of high atomic numbers are, in general, nonperturbative and a theoretical treatment based on a lowest-order Born approximation is insufficient. For the process of bound-free pair production at moderately relativistic impact energies, there has been some controversy as to the degree of failure of the Born approximation for the electron-positron interaction with the ''projectile ion'' (the latter defined as the ion which does not capture the electron) [3]. The basic reason why such controversy could build up and survive for an extended period of time is the computational difficulties involved in solving this collisional problem accurately.

As a background for the collisional problem we examine in this paper the related process of bound-free pair production following photon impact on a bare nucleus. Also this process is highly nonperturbative for high atomic numbers — although solely in the interaction with what would be the ''target ion'' in heavy-ion collisions. Furthermore, the photon induced process has the obvious advantage of being much easier to treat numerically than the collisional process. The results obtained for photon impact provide cross sections for not too close heavy-ion collisions through application of the Weizsäcker-Williams scheme of virtual quanta, which is perturbative in the projectile charge and, thereby, lead to reliable estimates for bound-free pair production for ion impact at ultrarelativistic energies.

The process of photon induced bound-free pair production was recently studied by Aste *et al.* [4], who gave total cross sections for production of K electrons. In the present paper [5], we shall basically confirm the results of these authors.

Furthermore, we shall discuss cross sections for production of L electrons, dependence on the positron emission angle for both shells and polarization effects. Throughout, we compare with results obtained in the Born approximation as well as with more accurate results obtained by other authors for related processes like, for instance, the photoelectric effect. We report results for a wide range of ion charges and photon energies. Towards the end, we shall comment briefly on the collisional case, where we note that the production of L electrons contribute significant probabilities for bound-free pair production.

II. TOTAL CROSS SECTION

The total cross section for photon induced bound-free pair production may be obtained by summing the partial cross sections for ending up in specific, scattering states, that is,

$$\sigma = \frac{1}{2} \sum_{\sigma, \lambda, m} \int d\Omega \, \frac{d\sigma(\vartheta, \phi)}{d\Omega}. \tag{1}$$

Alternatively, the sum may be taken over angular-momentum eigenstates (partial waves), so that,

$$\sigma = \frac{1}{2} \sum_{\lambda} \sum_{JLMm} \sigma_{JLM}. \tag{2}$$

In these equations λ and σ represent the helicities of the incoming photon and outgoing positron, respectively, m is the magnetic quantum number of the bound electron and J, L, and M are the angular-momentum quantum numbers of the partial wave. Obviously, σ is absent from Eq. (2) and J, L, and M from Eq. (1). Since the Coulomb-Dirac wave functions may only be obtained as a partial-wave expansion, the approach (2) is taken in this section.

The process of bound-free pair production may be viewed as the excitation of an electron from the negative-energy continuum to a bound state. Consequently, the partial cross section σ_{JLM} is similar to the usual photoabsorption cross

section given, for instance, by Bethe and Salpeter [6] and Merzbacher [7]; introducing the Compton wavelength λ_C, it becomes

$$\sigma_{JLM} = \frac{4\pi^2 \alpha}{k_0} |M|^2 \lambda_C^2. \qquad (3)$$

Here k_0 denotes the energy of the incoming photon which splits among the bound electron and the positron in amounts of E_b and $E_+ = k_0 - E_b$. The matrix element M is given as

$$M = M_{\lambda JLM} = \int d^3 \mathbf{r} \, \psi_b^\dagger(\mathbf{r}) \boldsymbol{\alpha} \cdot \mathbf{e}_\lambda e^{i\mathbf{k_0} \cdot \mathbf{r}} \psi_{JLM}(\mathbf{r}), \qquad (4)$$

where ψ_{JLM} is the appropriate negative continuum wave function and ψ_b is the wave function of the bound electron.

A. Wave functions

The wave function of a state characterized by the quantum numbers J, L, and M is given by

$$\psi_{JLM}(\mathbf{r}) = \begin{pmatrix} g_\kappa(r)\Omega_{JLM}(\vartheta,\phi) \\ if_\kappa(r)\Omega_{JL'M}(\vartheta,\phi) \end{pmatrix}, \qquad (5)$$

$$\Omega_{JLM} = \sum_{m_s = \pm 1/2} \langle L\tfrac{1}{2}M - m_s, m_s | L\tfrac{1}{2}JM \rangle$$
$$\times Y_{L,M-m_s}(\vartheta,\phi)\chi_{m_s}, \qquad (6)$$

where

$$\kappa = \mp(J + \tfrac{1}{2}), \quad L' = L \pm 1 \quad \text{for } J = L \pm \tfrac{1}{2}, \qquad (7)$$

$\langle \cdots | \cdots \rangle$ is a Clebsch-Gordan coefficient, Y_{LM} a spherical harmonic, and χ denotes a Pauli spinor. For actual calculations, the explicit expressions for the Ω's given by Greiner [8] are very convenient.

For point nuclei of charge Ze, the radial solutions for unbound states of energy E are given by the expressions

$$g_\kappa(r) = N_g (2pr)^{s-1}$$
$$\times \operatorname{Re}\{e^{i\delta}(s + i\eta)e^{-ipr}F(s + 1 + i\eta, 2s + 1, 2ipr)\}, \qquad (8)$$

$$f_\kappa(r) = N_f (2pr)^{s-1}$$
$$\times \operatorname{Im}\{e^{i\delta}(s + i\eta)e^{-ipr}F(s + 1 + i\eta, 2s + 1, 2ipr)\}, \qquad (9)$$

where $F(a,b,z) = {}_1F_1(a,b;z)$ as usual denotes the confluent hypergeometric function and the various parameters and normalization constants are given as

$$N_g = 2\left(\frac{pS_E(E+1)}{\pi}\right)^{1/2} e^{\pi\eta/2} \frac{|\Gamma(s + i\eta)|}{\Gamma(2s + 1)}, \qquad (10)$$

$$N_f = -N_g S_E \left(\frac{E-1}{E+1}\right)^{1/2},$$

$$p = \sqrt{E^2 - 1}, \quad \eta = \frac{\alpha ZE}{p}, \quad e^{2i\delta} = \frac{-\kappa + i\eta/E}{s + i\eta}, \qquad (11)$$

$$s = \sqrt{\kappa^2 - \alpha^2 Z^2}, \quad S_E = \frac{E}{|E|}.$$

In these equations, $\alpha \simeq 1/137$ is the fine-structure constant, and, as in the rest of this paper, the electron mass, the speed of light, and $\hbar$ is set to unity.

The wave functions for bound motion around point nuclei may also be written in the form (5), but in this case, the radial functions read

$$g_\kappa(r) = N_b r^{s-1} e^{-p_0 r}$$
$$\times \left\{ \left(\frac{(n'+s)}{E} - \kappa\right) F(-n', 2s + 1, 2p_0 r) \right.$$
$$\left. - n'F(1 - n', 2s + 1, 2p_0 r) \right\}, \qquad (12)$$

$$f_\kappa(r) = -\left(\frac{1-E}{1+E}\right)^{1/2} N_b r^{s-1} e^{-p_0 r}$$
$$\times \left\{ \left(\frac{(n'+s)}{E} - \kappa\right) F(-n', 2s + 1, 2p_0 r) \right.$$
$$\left. + n'F(1 - n', 2s + 1, 2p_0 r) \right\}, \qquad (13)$$

where

$$N_b = \frac{(2p_0)^{s+1/2}}{\Gamma(2s + 1)} \left(\frac{(1 + E)\Gamma(2s + n' + 1)}{4n'/E} \right)^{1/2}, \qquad (14)$$

$$E = \left[1 + \frac{(\alpha Z)^2}{(n - |\kappa| + s)^2} \right]^{-1/2}, \quad p_0 = \sqrt{1 - E^2}, \quad n' = n - |\kappa|, \qquad (15)$$

while s and κ are as defined above and n denotes the main quantum number. The expressions for the lowest shells are actually quite simple. For the ground state, for example, we have

$$g_\kappa(r) = N_0 r^{s_{1s}-1} e^{-\alpha Zr}, \quad f_\kappa(r) = -\left(\frac{1 - s_{1s}}{1 + s_{1s}}\right)^{1/2} g_\kappa(r), \qquad (16)$$

where N_0 turns out to be

$$N_0 = (2\alpha Z)^{s_{1s}+1/2} \left(\frac{1 + s_{1s}}{2\Gamma(2s_{1s} + 1)}\right)^{1/2}. \qquad (17)$$

B. Matrix elements

In preparation for the numerical work, we now derive formulas for the matrix elements between bound states and free spherical waves. The bound state of energy E_b is characterized by the quantum numbers j, l, and m, while the positron is represented by a negative-energy solution to the Dirac equation for the Coulomb potential, characterized by the energy $E = -E_+ = E_b - k_0$ and the quantum numbers J, L, and M.

In the following calculation, let us choose the polarization vector $\mathbf{e}_\lambda$ to correspond to a photon of positive helicity, that is, $\lambda = +$. Inserting Eq. (5) in the expression for the matrix element then yields $[\kappa_b = \mp (j + \frac{1}{2})]$

$$M = i \int d^3\mathbf{r} e^{i\mathbf{k_0}\cdot r}[g_{\kappa_b}(r)f_\kappa(r)\Omega^\dagger_{jlm}\sigma_+\Omega_{JL'M}$$
$$- f_{\kappa_b}(r)g_\kappa(r)\Omega^\dagger_{jl'm}\sigma_+\Omega_{JLM}], \quad (18)$$

where

$$\sigma_+ = \begin{pmatrix} 0 & \sqrt{2} \\ 0 & 0 \end{pmatrix}. \quad (19)$$

In order to do the integral, $\mathbf{k}_0$ is assumed to be in the direction of the z axis, which allows us to write $\mathbf{k}_0 = k_0\mathbf{e}_z$ and use the expansion

$$e^{ik_0 z} = \sum_{k=0}^\infty i^k\sqrt{4\pi(2k+1)}j_k(k_0 r)Y_{k0}(\vartheta,\phi), \quad (20)$$

where j_k, as usual, denotes a spherical Bessel function. Inserting this and exchanging the order of integration and summation enables us to express the matrix element as the following sum of integrals:

$$M = \sum_{k=0}^\infty i^{k+1}[I_1^{(k)} - I_2^{(k)}], \quad (21)$$

where

$$I_1^{(k)} = \sqrt{4\pi(2k+1)}\int_0^\infty dr\ r^2 j_k(k_0 r)$$
$$\times g_{\kappa_b}(r)f_\kappa(r)\int d\Omega\ \Omega^\dagger_{jlm}\sigma_+\Omega_{JL'M}Y_{k0}, \quad (22)$$

$$I_2^{(k)} = \sqrt{4\pi(2k+1)}\int_0^\infty dr\ r^2 j_k(k_0 r)$$
$$\times f_{\kappa_b}(r)g_\kappa(r)\int d\Omega\ \Omega^\dagger_{jl'm}\sigma_+\Omega_{JLM}Y_{k0}. \quad (23)$$

The integrals (22) and (23) separate into radial and angular parts. We write

$$I_i^{(k)} = I_{i,\vartheta}^k I_{i,r}^{(k)}, \quad i = 1,2, \quad (24)$$

and include the square root in the angular integral.

Only a finite amount of the terms in Eq. (21) do, in fact, contribute to the sum due to angular selection rules. As an example, consider the integral I_1. With the definition

$$C_{jlm}^{JLM}$$
$$= \begin{cases} \sqrt{2(j+m)(J-M)} & j=l+\frac{1}{2}, \quad J=L+\frac{1}{2} \\ \sqrt{2(j+m)(J+M+1)} & j=l+\frac{1}{2}, \quad J=L-\frac{1}{2} \\ -\sqrt{2(j-m+1)(J-M)} & j=l-\frac{1}{2}, \quad J=L+\frac{1}{2} \\ -\sqrt{2(j-m+1)(J+M+1)} & j=l-\frac{1}{2}, \quad J=L-\frac{1}{2} \end{cases}$$

the angular part may be written as

$$I_{1,\vartheta}^{(k)} = \left(\frac{4\pi(2k+1)}{(2l+1)(2L+1)}\right)^{1/2}$$
$$\times C_{jlm}^{JLM}\int d\Omega\ Y^*_{l,m-1/2}Y_{L',M+1/2}Y_{k0}. \quad (26)$$

From the selection rules for the Clebsch-Gordan coefficients it follows that this matrix element vanishes identically unless $M = m - 1$, unless $|l - L'| \leq k \leq l + L'$ and unless $l + L' + k$ is an even number.

For bound s states, the summation over k in Eq. (21) may be performed to yield the following result ($J = L \pm \frac{1}{2}$):

$$M = i^{L'+1}\sqrt{2J+1}\left[I_{1,r}^{(L')} \mp \frac{L-1}{2L+1}I_{2,r}^{(L-1)} \pm \frac{L}{2L+1}I_{2,r}^{(L+1)}\right],$$
$$m = +\frac{1}{2},$$

$$M = i^L\sqrt{2J+1}\pm 2\frac{\sqrt{L(L+1)}}{2L+1}[I_{2,r}^{(L+1)} + I_{2,r}^{(L-1)}],$$
$$m = -\frac{1}{2}. \quad (27)$$

The result for bound $p_{1/2}$ states follows by interchanging L and L', I_1 and I_2. For bound $p_{3/2}$ states, the angular integrals read

$$I_{1,\vartheta}^{(k)} = (-1)^{m-1/2}(2k+1)C_{(3/2)1m}^{JL'm-1}\begin{pmatrix} 1 & L' & k \\ -m+\frac{1}{2} & m-\frac{1}{2} & 0 \end{pmatrix}$$
$$\times\begin{pmatrix} 1 & L' & k \\ 0 & 0 & 0 \end{pmatrix}, \quad (28)$$

$$I_{2,\vartheta}^{(k)} = (-1)^{m-1/2}(2k+1)C_{(3/2)2m}^{JLm-1}\begin{pmatrix} 2 & L & k \\ -m+\frac{1}{2} & m-\frac{1}{2} & 0 \end{pmatrix}$$
$$\times\begin{pmatrix} 2 & L & k \\ 0 & 0 & 0 \end{pmatrix}, \quad (29)$$

which may be computed by use of the relations for the $3j$ symbols given by Sobel'man [9] together with their symmetry properties, see also Weissbluth [10]. The actual calculation would, of course, be the same as for the s state, only now we have four possible values of the quantum number m and some slightly more complicated $3j$ symbols.

The radial integrals (22)–(24) may be written as

$$I_{1,r}^{(k)} = N_f (2p)^{s-1} \, \text{Im}\left\{ e^{i\delta}(s+i\eta) \int_0^\infty dr \; r^{s+1} e^{-ipr} j_k(k_0 r) \right.$$

$$\left. \times g_b(r) F(s+1+i\eta, 2s+1, 2ipr) \right\}, \tag{30}$$

$$I_{2,r}^{(k)} = N_g (2p)^{s-1} \, \text{Re}\left\{ e^{i\delta}(s+i\eta) \int_0^\infty dr \; r^{s+1} e^{-ipr} j_k(k_0 r) \right.$$

$$\left. \times f_b(r) F(s+1+i\eta, 2s+1, 2ipr) \right\}, \tag{31}$$

where index b is used for the bound state; the parameter s (as well as parameters p, η, and δ) relates to the continuum state. The integrals (30) always involve sums of integrals of the same type, since all bound-state wave functions are of the form of a polynomial times a power times an exponential. Hence, we shall start focusing on the ground-state integrals, since this will demonstrate all nontrivial aspects of the calculations.

Inserting the ground-state wave function (16) in Eq. (30) above, we obtain

$$I_{1,r}^{(k)} = N_f N_0 (2p)^{s-1} \text{Im}\{ e^{i\delta}(s+i\eta) K(s, s_{1s}, k, \alpha Z, p, k_0) \}, \tag{32}$$

$$I_{2,r}^{(k)} = -N_g N_0 \left(\frac{1-s_{1s}}{1+s_{1s}} \right)^{1/2} (2p)^{s-1} \text{Re}\{ e^{i\delta}(s+i\eta) \right.$$

$$\left. \times K(s, s_{1s}, k, \alpha Z, p, k_0) \}, \tag{33}$$

with K defined as

$$K(s, s_b, k, p_0, p, k_0) = \int_0^\infty dr \; r^{s+s_b} e^{-(p_0+ip)r} j_k(k_0 r)$$

$$\times F(s+1+i\eta, 2s+1, 2ipr). \tag{34}$$

Various approaches may be taken in order to evaluate this integral. The approach to be taken here is similar to the method of [11] and also used in [12] as well as in [13]. It consists of expressing the spherical Bessel function of the integrand as a finite sum of exponentials, that is,

$$j_k(z) = \sum_{\iota=0}^{k} \frac{(k+\iota)!}{\iota!(k-\iota)!} i^{k+1-\iota} (2z)^{-\iota-1}$$

$$\times [(-1)^{k+1-\iota} e^{iz} + e^{-iz}]. \tag{35}$$

Insertion of this expression reduces Eq. (34) to

$$K(s, s_b, k, p_0, p, k_0) = \sum_{\iota=0}^{k} \frac{(k+\iota)!}{\iota!(k-\iota)!} i^{k+1-\iota} (2k_0)^{(-\iota-1)}$$

$$\times [(-1)^{k+1-\iota} \widetilde{I}^- + \widetilde{I}^+], \tag{36}$$

with the definition

$$\widetilde{I}^{\pm} = \int_0^\infty dr \; r^{s+s_b-1-\iota} e^{-[p_0+i(p\pm k_0)]r}$$

$$\times F(s+1+i\eta, 2s+1, 2ipr). \tag{37}$$

We will first examine $\widetilde{I}^+$, since it turns out to be the simplest. We introduce an integral representation of the confluent hypergeometric function,

$$F(a,b,z) = \frac{\Gamma(b)}{\Gamma(a)\Gamma(b-a)} \int_0^1 du \; u^{a-1}(1-u)^{b-a-1} e^{zu}, \tag{38}$$

in Eq. (37) whereby

$$\widetilde{I}^+ = \frac{\Gamma(2s+1)}{\Gamma(s+1+i\eta)\Gamma(s-i\eta)} \int_0^1 du \; u^{s+i\eta}(1-u)^{s-i\eta-1}$$

$$\times \int_0^\infty dr \; r^{s+s_b-1-\iota} e^{-(p_0+i[p(1-2u)+k_0]r)}. \tag{39}$$

Upon elementary substitutions, the r integral yields a Γ function [14]

$$\widetilde{I}^+ = \frac{\Gamma(s+s_b-\iota)\Gamma(2s+1)}{\Gamma(s+1+i\eta)\Gamma(s-i\eta)} \int_0^1 du \; u^{s+i\eta}(1-u)^{s-i\eta-1}$$

$$\times \{ p_0 + i[p(1-2u)+k_0] \}^{\iota-s-s_b}. \tag{40}$$

If we now rewrite the factor in the integrand involving p, p_0, and k_0, making use of the simple algebraic fact

$$p_0 + i[p(1-2u)+k_0] = [p_0 + i(p+k_0)]\left(1 - \frac{2pu}{p+k_0-ip_0} \right), \tag{41}$$

the remaining integral over u may conveniently be expressed in terms of the integral representation of the (nondegenerate) hypergeometric function

$$F(a,b;c;z) = {}_2F_1(a,b;c;z)$$

$$= \frac{\Gamma(c)}{\Gamma(a)\Gamma(c-a)} \int_0^1 du \; u^{a-1}(1-u)^{c-a-1}$$

$$\times (1-zu)^{-b}. \tag{42}$$

Upon comparison, we obviously have

$$\widetilde{I}^+ = \frac{\Gamma(s+s_b-\iota)}{[p_0+i(p+k_0)]^{s+s_b-\iota}}$$

$$\times F\left(s+1+i\eta, s+s_b-\iota; 2s+1; \frac{2p}{p+k_0-ip_0} \right). \tag{43}$$

As for $\widetilde{I}^-$, we will first apply the Kummer transformation $F(a,b,z) = e^z F(b-a,b,-z)$ whereby we may write

$$\widetilde{I}^- = \frac{\Gamma(s+s_b-\iota)}{[p_0-i(p+k_0)]^{s+s_b-\iota}}$$

$$\times F\left(s-i\eta, s+s_b-\iota; 2s+1; \frac{2p}{p+k_0+ip_0} \right). \tag{44}$$

To summarize, the radial integrals for the ground state, of energy $E_{1s}=s_1=\sqrt{1-(\alpha Z)^2}$, are given by Eqs. (32) and (33), with K given by Eqs. (36) and (43)–(44); see also [15].

Let us now turn to the L shell. For the $2p_{3/2}$ state of energy $E_{2p_{3/2}}=s_2/2=\sqrt{1-(\alpha Z/2)^2}$ we get

$$I_{1,r}^{(k)}=N_f N_{2p_{3/2}}(2p)^{s-1}$$
$$\times \mathrm{Im}\{e^{i\delta}(s+i\eta)K(s,s_2,k,\alpha Z/2,p,k_0)\}, \quad (45)$$

$$I_{2,r}^{(k)}=-\left(\frac{1-E_{2p_{3/2}}}{E_{2p_{3/2}}+1}\right)^{1/2}N_g N_{2p_{3/2}}(2p)^{s-1}$$
$$\times \mathrm{Re}\{e^{i\delta}(s+i\eta)K(s,s_2,k,\alpha Z/2,p,k_0)\}. \quad (46)$$

The integrals corresponding to the $2s$ and $2p_{1/2}$ states, which have the same energy $E_{2s}=E_{2p_{1/2}}=\sqrt{(1+s_1)/2}$, are slightly more complicated. By introduction of the quantities

$$K_1=K(s,s_1,k,p_0,p,k_0), \quad K_2=K(s,s_1+1,k,p_0,p,k_0), \quad (47)$$

where now $p_0=\sqrt{(1-s_1)/2}$, we get for the $2s$ state

$$I_{1,r}^{(k)}=N_f N_{2s}(2p)^{s-1}$$
$$\times \mathrm{Im}\left\{e^{i\delta}(s+i\eta)\left[2E_{2s}K_1-\frac{2p_0}{2E_{2s}-1}K_2\right]\right\}, \quad (48)$$

$$I_{2,r}^{(k)}=-\left(\frac{1-E_{2s}}{E_{2s}+1}\right)^{1/2}N_g N_{2s}(2p)^{s-1}$$
$$\times \mathrm{Re}\left\{e^{i\delta}(s+i\eta)\left[(2E_{2s}+2)K_1-\frac{2p_0}{2E_{2s}-1}K_2\right]\right\}. \quad (49)$$

And, very similarly, for $2p_{1/2}$

$$I_{1,r}^{(k)}=N_f N_{2p_{1/2}}(2p)^{s-1}$$
$$\times \mathrm{Im}\left\{e^{i\delta}(s+i\eta)\left[(2E_{2p_{1/2}}-2)K_1-\frac{2p_0}{2E_{2p_{1/2}}+1}K_2\right]\right\}, \quad (50)$$

$$I_{2,r}^{(k)}=-\left(\frac{1-E_{2p_{1/2}}}{E_{2p_{1/2}}+1}\right)^{1/2}N_g N_{2p_{1/2}}(2p)^{s-1}$$
$$\times \mathrm{Re}\left\{e^{i\delta}(s+i\eta)\left[2E_{2p_{1/2}}K_1-\frac{2p_0}{2E_{2p_{1/2}}+1}K_2\right]\right\}. \quad (51)$$

To summarize, the radial integrals for the L shell are given by Eqs. (45)–(51) with K again given by Eq. (36) and Eqs. (43) and (44).

C. Numerical results

The perturbation result for the total cross section for pair production with capture to the K shell may be obtained from
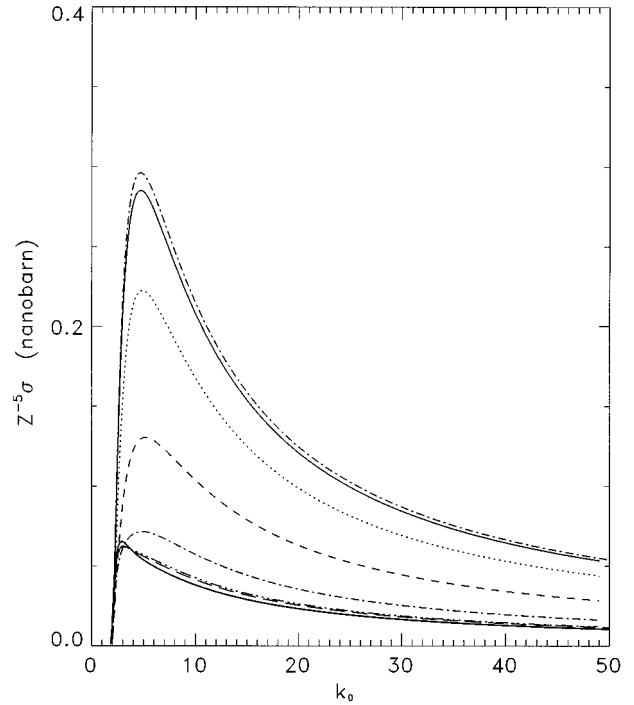

FIG. 1. Total cross section for pair production with the electron bound in the $1s$ state as a function of photon energy for nuclear charge numbers Z of 1 (upper full-drawn curve), 8 (dotted), 26 (short dashes), 55 (dotted-dashed), 79 (triple-dotted-dashed), 82 (long dashes), and 92 (lower full-drawn curve). Cross sections are scaled with Z^5, the unit on the ordinate is 10^{-33} cm^2, and the photon energy is given in units of mc^2, the electron rest energy. The uppermost curve (dotted-dashed) corresponds to the Born result (52).

Sauter's Born-approximation result for the photoelectric effect [16] by performing appropriate substitutions. It reads

$$\sigma_B=4\pi\lambda_C^2\alpha(\alpha Z)^5\frac{p^3}{k_0^5}$$
$$\times\left(\frac{4}{3}+\frac{E_+(E_+-2)}{E_++1}\left[1-\frac{1}{2E_+p}\ln\left(\frac{E_++p}{E_+-p}\right)\right]\right), \quad (52)$$

where E_+ as usual denotes the positron energy, p is the positron momentum, and k_0 the photon momentum (that is, the photon energy). In the extreme high-energy limit, Eq. (52) reduces to the so-called Sauter cross section

$$\sigma_0=\frac{4\pi\alpha(\alpha Z)^5}{k_0}\lambda_C^2, \quad (53)$$

which also applies for the photoelectric effect. The Born results (52) and (53) are valid for $\alpha Z\ll 1$ and show a scaling with Z^5. Hence we expect a moderate variation with nuclear charge if we divide exact cross sections with Z^5.

Figure 1 shows the K-shell cross section scaled with Z^5 as a function of photon energy for seven elements together with the Born result (52). The curves in Fig. 1 all show a peak at low photon energies followed by a decrease which approaches the asymptotic $1/k_0$ dependence at high energies, cf. Eq. (53). The shapes for different Z are rather similar, but the peaking appears at lower energies for higher charges. The
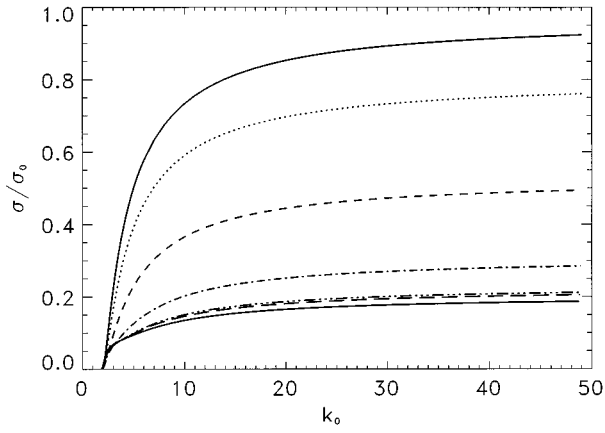
FIG. 2. Ratio of the exact cross sections displayed in Fig. 1 to the Sauter cross section (53). The charge numbers and symbols used are the same as in Fig. 1.

TABLE I. Comparison between the high-energy limits of σ/σ_0 for the K shell extrapolated from the present work and those given by Pratt [17], the high-energy approximation (55) obtained by Aste *et al.* [4], and the modified Hall formula (56). The numbers marked with an asterisk are extrapolated from the data given by Pratt, Ron, and Tseng [22].

Z	Present	Pratt	(55)	(56)
92	0.196	0.203	0.182	0.175
82	0.216	0.223	0.197	0.201
79	0.222	0.228*	0.203	0.209
55	0.293	0.310*	0.271	0.305
26	0.518	0.532*	0.4875	0.529
8	0.798	0.793*	0.784	0.805
1	0.971		0.969	0.972

absolute values for unit nuclear charge are close to the Born result (52), but as Z increases, values become lower corresponding to a slower Z dependence of the cross section than the perturbative Z^5 scaling.

It may be noted that near threshold, bound-free pair production dominates over free-free pair production. For the case of $Z=92$, this holds true for nearly all of the first energy unit beyond threshold. Right after curves cross, the bound-free cross section goes through its maximum while the cross section for production of free pairs continues to increase steeply.

The dependence of K-shell cross sections on energy and charge is further illustrated in Fig. 2, which shows the cross sections of Fig. 1 in units of the Sauter cross section (53). Plotted in this way, each curve tends to a constant at high energies so that, following Pratt [17] and Milstein and Strakhovenko [18], we may write the high-energy cross section as

$$\sigma_K = \sigma_0 f(Z), \quad k_0 \to \infty. \tag{54}$$

From the plot we see that $f(Z)$ is a decreasing function of Z, and we further note that the high-energy limit is essentially reached at the maximum energy displayed (25 MeV). Aste *et al.* [4] have suggested a ''purely heuristic'' formula for $f(Z)$,

$$f(Z) = \left(\frac{1}{2} + \frac{\alpha Z}{4} \right)^{2\pi\alpha Z}. \tag{55}$$

Even though our results are in good agreement with those of [4], this formula turns out to be somewhat below the mark (5–10%). The numerical high-energy results of Pratt [17], obtained in studies of the photoelectric effect, are in better agreement with the present calculations. Another useful approximation formula is the modified Hall formula [17]

$$\sigma = \sigma_0 (\alpha Z)^{2\xi} e^{-2\alpha Z \cos^{-1}\alpha Z} (1 - 4\pi\alpha Z/15), \tag{56}$$

where $\xi = s_1 - 1 = \sqrt{1 - (\alpha Z)^2} - 1$ ($\approx -\alpha^2 Z^2/2$); see also [19]. The various results for $f(Z)$ are compared in Table I. The formulas (55) and (56) are seen to be of nearly the same quality. The discrepancies between our high-energy limits

[21] and those given in [22] may well be caused by inaccuracies in the original calculations of Pratt [17]; obviously, a lot has happened in the realm of electronic computers since 1960, and an attempt to repeat the computation of the exact high-energy limit might not be superfluous, especially since the method used by Pratt did not permit him to perform the calculations in the low-Z limit. It may be noted, that for energies beyond ca. 20 electron masses, there is a good agreement between the present results and those of a modified Born approximation, obtained by multiplying the Born result (52) by the numerically obtained $f(Z)$.

Figure 3 illustrates the distribution of the cross section over angular momenta J of the positron. With increasing energy, the number of partial waves that contribute to the total cross section gets higher; on the figure we show the contributions for $J \leqslant 100$, but for a positron of energy $25mc^2$ it is actually necessary to include the contributions up to, roughly, $J = 200$ in order to get a sufficiently accurate result. A very conspicuous feature of the distribution of the cross section on the angular-momentum quantum numbers at moderate and high energies is the sharp peak at low J, fol-
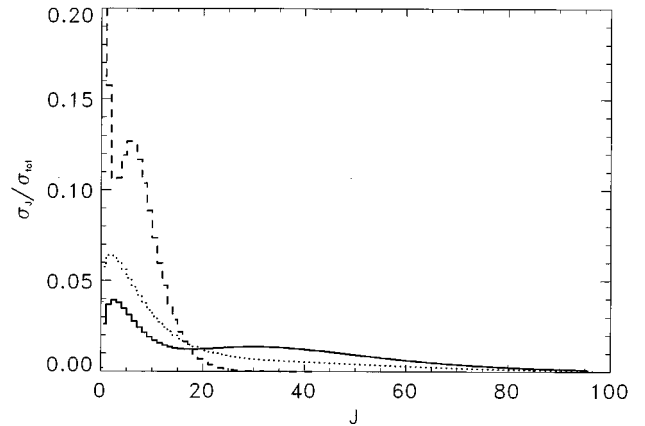

FIG. 3. Partial cross sections for pair production on a bare lead nucleus with the electron bound in the $1s$ state. The contributions σ_J from the individual partial waves of total angular momentum J are shown in units of the total cross section. The full-draw histogram corresponds to a positron energy of $25mc^2$, while the dashed is for $5mc^2$. For comparison, the dotted histogram displays the result for $Z=1$ at the higher energy.
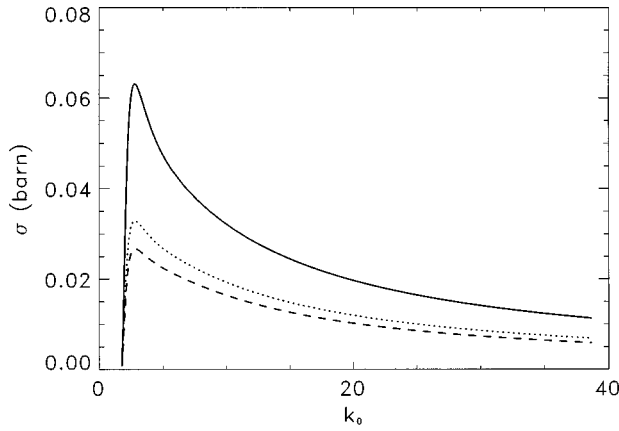
FIG. 4. Cross sections for pair production with capture to the $2s_{1/2}$ shell as a function of photon energy in units of mc^2 for $Z=92$ (full curve), 82 (dotted), and 79 (dashed).

lowed by a decrease and a new increase producing a local maximum at higher J. The peak at low J is the contribution from the radial integral I_1 containing the large components of the wave functions, whereas the local maximum at high J stems from the integral I_2 containing the small components. In the low-Z limit the contribution from I_2 tends to vanish, and, indeed, the local maximum at high J is missing on the histogram displayed in the figure for $Z=1$.

As proved, e.g., by Pratt [23], to first order in αZ the ns-shell cross sections obey a scaling law, so that

$$\sigma_{ns} = \frac{1}{n^3} \sigma_K. \qquad (57)$$

Furthermore, Gavrila's second-order Born approximation for the $2s$ state yielded identically $1/8$ of his second-order K-shell cross section [24]. Calculations by Pratt showed that in the high-energy limit, the n^{-3} scaling is very close to the exact result not only at low charge numbers but in general at all values of Z. The $2p$ states, on the other hand, have quite insignificant cross sections at low target charges while at high target charges they will be of the same order of magnitude as the $2s$ cross sections (though still smaller). In the Born approximation, that is, to lowest order in αZ, cross sections for p states are expected to increase in proportion to Z^7 as compared to Z^5 for s states, cf. [24]. The result is that the cross section for bound-free pair production with capture to the L shell is approximately 12.5% of the K-shell cross section for low target charges, where the Born approximation is valid, and about 20% for high target charges. The present calculations show that this prediction, which was originally based on Pratt's high-energy calculations, is valid at practically all energies away from threshold. Figures 4 and 5 show the contributions from the $2s$ states and the $2p_{1/2}$ states for three heavy elements. For these high-Z targets contributions from the $2p_{1/2}$ states are about half of those from the $2s$ states. In Fig. 6, we show the lower $2p_{3/2}$ cross sections for the same three elements. By comparing Figs. 5 and 6 to Fig. 4, the increasing importance of p states with increasing Z is evident. We also mention that for $Z=1$, where the p-state contribution to the total L-shell cross section is very small, our results for the two $2p$ states are in good agreement with
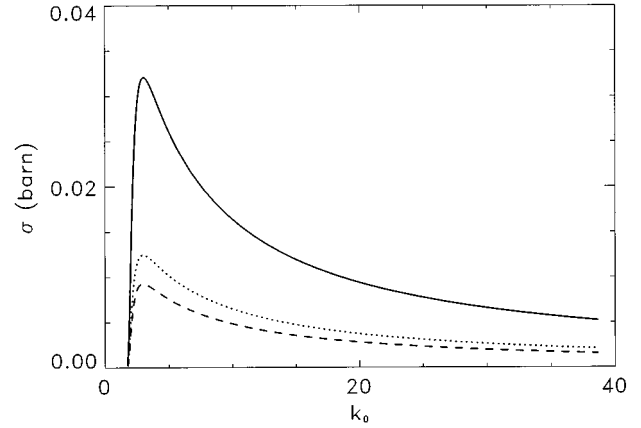
those presented in [24]; for the $2p_{1/2}$ state, which at low Z actually makes the smallest contribution of the two, the agreement is even very close.

Figure 7 displays the ratios of cross sections to the K-shell cross section for the three L states as well as for the entire L shell for the three heavy targets selected in Figs. 4–6. At energies beyond 5 units, all ratios are essentially constant. The $2s$ curves all saturate at a level close to the value $1/8$. The $2p_{1/2}$ curves, on the other hand, show significant Z dependence, even faster than the $Z^7/Z^5=Z^2$ prediction of the Born approximation, whereas the $2p_{3/2}$ ratios only depend weakly on Z. Due to the Z dependence of the $2p_{1/2}$ results, also the ratio for the entire L shell shows some Z dependence with asymptotic ratios ranging from 18% to 21% for the three selected heavy targets (again to be compared with 12.5% in the low-Z limit).

The high-energy limit for the L-shell cross sections is most easily obtained by applying the high-energy values for the shell ratios and Eqs. (54) and (53) for the K-shell cross section with $f(Z)$ taking values according to Table I. The shell ratios obtained in our calculation are displayed in Table II and compared to results obtained by Pratt [23].

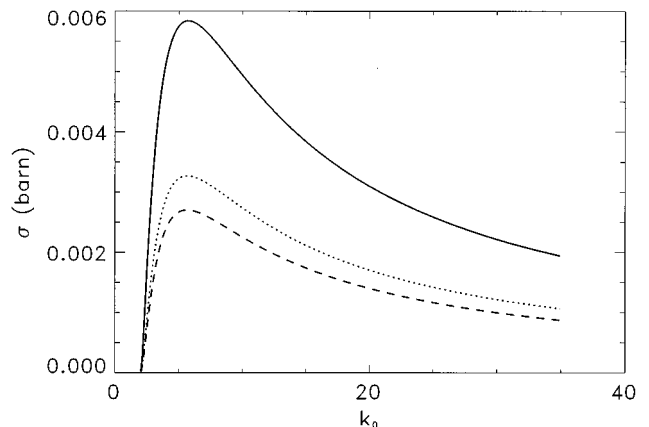Total cross sections for bound-free pair production by

FIG. 6. Cross sections for pair production with capture to the $2p_{3/2}$ shell as a function of photon energy in units of mc^2 for $Z=92$ (full curve), 82 (dotted), and 79 (dashed).

FIG. 5. Cross sections for pair production with capture to the $2p_{1/2}$ shell as a function of photon energy in units of mc^2 for $Z=92$ (full curve), 82 (dotted), and 79 (dashed).
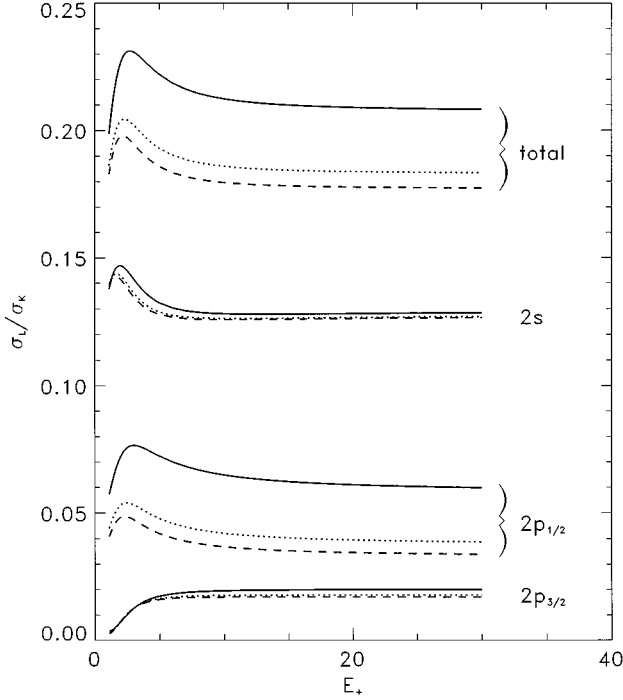
FIG. 7. Shell ratios. The ratios of cross sections for pair production with capture into the individual L subshells to the cross section for capture into the K shell are shown as functions of positron energy in units of mc^2 for three different elements; $Z=92$ (full curve), 82 (dotted), and 79 (dashed). The three close-lying curves at the bottom of the figure display results for the $2p_{3/2}$ state, then follow the three curves for the $2p_{1/2}$ state, the close packed group of curves for the $2s$ state and, at the top of the figure, the sum of the partial ratios.

high-energy photons where the electron ends up in the M or any higher shell are given in [18]. According to [18], the contribution from M and higher shells amounts to approximately 60% of the L-shell contribution for all charge numbers.

III. DIFFERENTIAL CROSS SECTIONS

In order to obtain differential cross sections, the continuum state of an electron is represented by a scattering state $\Psi^{\pm}$ corresponding to an incoming (outgoing) plane wave plus outgoing (incoming) spherical waves. Relativistic Coulomb scattering states are only available in a partial-wave expansion. This is given by Rose [25] and may be written

$$\Psi^{\pm}=4\pi\left(\frac{\pi}{2Ep}\right)^{1/2}\sum_{JLM} i^L e^{\pm i\delta_\kappa}$$

$$\times\langle L\tfrac{1}{2}(M-\tfrac{1}{2}\sigma)\tfrac{1}{2}\sigma|L\tfrac{1}{2}JM\rangle$$

$$\times Y^*_{L,M-\sigma/2}(\hat{\mathbf{p}})\psi_{JLM}(\mathbf{r}), \tag{58}$$

where ψ_{JLM} are the partial waves listed in Sec. II A and δ_κ is the Coulomb phase shift, given by

$$\delta_\kappa=\delta+(L+1-s)\frac{\pi}{2}-\text{arg}\{\Gamma(s+i\eta)\}. \tag{59}$$

To describe an outgoing positron of momentum $\mathbf{p}$ and helicity σ we make the substitutions $\mathbf{p}\to-\mathbf{p}$ and $\sigma\to-\sigma$ in Eq. (58) and select the incoming wave; that is, we consider the state

$$\Psi_{\mathbf{p}}^{-}=4\pi\left(\frac{\pi}{2Ep}\right)^{1/2}\sum_{JLM} i^L e^{-i\delta_\kappa}$$

$$\times\langle L\tfrac{1}{2}(M+\tfrac{1}{2}\sigma)\tfrac{1}{2}\sigma|L\tfrac{1}{2}JM\rangle$$

$$\times Y^*_{L,M+\sigma/2}(-\hat{\mathbf{p}})\psi_{JLM}(\mathbf{r}). \tag{60}$$

The differential cross section then reads

$$\frac{d\sigma}{d\Omega}=\frac{\alpha pE_+}{2\pi k_0}|\widetilde{M}|^2, \tag{61}$$

where E_+ denotes the energy of the emitted positron and E_b the bound-state energy. The matrix element is given as

$$\widetilde{M}=\int d^3r\,\psi_b^{\dagger}(\mathbf{r})\boldsymbol{\alpha}\cdot\mathbf{e}_\lambda e^{i\mathbf{k_0}\cdot\mathbf{r}}\Psi_{\mathbf{p}}^{-}$$

$$=4\pi\left(\frac{\pi}{2E_+p}\right)^{1/2}\sum_{JLM} i^L e^{-i\delta_\kappa}$$

$$\times\langle L\tfrac{1}{2}(M+\tfrac{1}{2}\sigma)\tfrac{1}{2}\sigma|L\tfrac{1}{2}JM\rangle$$

$$\times Y^*_{L,M+\sigma/2}(-\hat{\mathbf{p}})M_{\lambda JLM}, \tag{62}$$

where $M_{\lambda JLM}$ are the partial-wave matrix elements introduced in Sec. II.

A. Numerical results

Figure 8 displays the differential cross section for pair production with the produced electron bound in the K shell

TABLE II. High-energy limits of the ratios of cross sections for the various L subshells to the cross section for the K shell. The results marked with superscript P are the high-energy results listed in [23], except for the case $Z=1$, where the high-energy limit of Gavrila's Born approximation is used [24]. As in Table I, the asterisk indicates that results are extrapolated from the data given in [22].

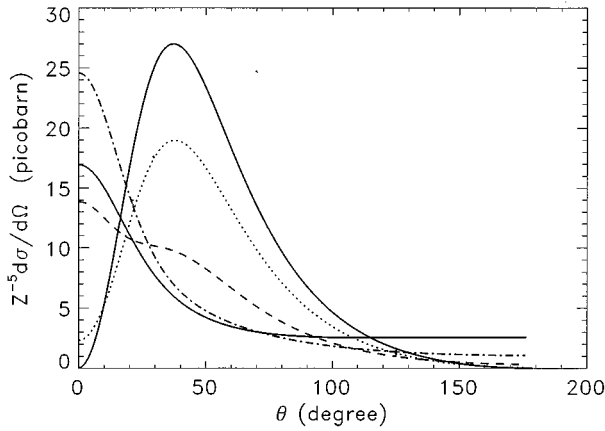| Z	$2s$	$2s^P$	$2p_{1/2}$	$2p_{1/2}^P$	$2p_{3/2}$	$2p_{3/2}^P$
92	0.129	0.130	0.0598	0.0576	0.0201	0.0212
82	0.128	0.128	0.0385	0.0374	0.0178	0.0179
79	0.127	0.127*	0.0340	0.0331*	0.0171	0.0165*
1	0.125	0.125	1.24×10^{-6}	1.25×10^{-6}	4.24×10^{-6}	4.44×10^{-6}

FIG. 8. Angular distribution of positrons at an energy of $1.5mc^2$ for pair production with K-shell capture at targets of charge numbers for $Z=1$ (full curve), 8 (dotted), 26 (dashed), 55 (chained), and 92 (full, with a maximum in the forward direction). The differential cross sections are scaled by Z^5 and the ordinate is given in units of 10^{-36} cm^2 per steradian.

FIG. 10. Angular distribution of positrons at an energy of $1.5mc^2$ for pair production with L-shell capture. The upper full-drawn curve is for production of $2s$ electrons on a target nucleus with $Z=92$, the close-lying dotted curve is 1/8 times the corresponding K-shell result, cf. Fig. 8. The three lower curves are for production of electrons in the $2p_{1/2}$ state around nuclei with charge numbers numbers for $Z=92$ (full curve), 82 (dotted), and 79 (dashed). The unit on the ordinate is 10^{-24} cm^2 per steradian.

and the positron emitted with a total energy of $1.5mc^2$ for five different target elements. At low target charges the differential cross section vanishes in the forward direction. This is in agreement with the prediction of the Born approximation; see also [26]. At high charges, on the other hand, the angular distributions show a maximum in the forward direction. The transition from the low-Z to the high-Z behavior takes place already at moderate charge numbers; for $Z=8$, the value for forward emission is distinct from zero and at $Z=26$ the global maximum is at zero angle. It may be noted that at low Z, but not moderate and high Z, our angular distribution is quite similar to that of the K-shell photoelectric effect, which for any charge number has a local minimum in the forward direction [12]. On the other hand, for

single-quantum annihilation a maximum is encountered in the forward direction at high Z [27] as we find it for the bound-free pair production.

Figure 9 displays the angular distributions at higher energies for a heavy target element as well as for unit nuclear charge. With the abscissa chosen as the product of positron energy and emission angle, the curves are all confined within a few units corresponding to a scaling of characteristic angles with the inverse of the positron energy E_+. When this result is combined with the asymptotic $1/E_+$ dependence of the total cross section it is obvious, that the differential cross sections scale roughly with E_+. Accordingly, as ordinate in Fig. 9 we have used differential cross section divided by energy as well as by Z^5. Plotted in this way, the shapes of the curves for a given element are similar at all energies and the variation in absolute values is moderate.

Figure 10 displays the differential cross section for production of the electron in the $2s$ and $2p_{1/2}$ states at a low energy. The result for the $2s$ state, which is shown for $Z=92$, is close to one-eighth of the corresponding K-shell result, which is also shown. The form of the angular distributions for the $2p_{1/2}$ state, shown for three different heavy elements, is quite similar to that of the s state, though a little broader, but the Z dependence is stronger. This similarity in shapes between the s and p distributions does not appear at low charge numbers. At $Z=1$, the result for the $2p_{1/2}$ state is still at maximum in the forward direction, see also [24], while the result for the s state essentially vanishes here. It may be noted, however, that the s results do not exactly vanish in the forward direction for low Z, and due to the suppression of the p results at all angles for low Z, the s results still superseed the p results for forward emission.

Figure 11 shows the differential cross section for production of $2p_{1/2}$ electrons at a high energy for three high-Z targets as well as for $Z=1$. The result for the $2s$ state is not shown as it is again close to one-eighth of the K-shell result for all Z.
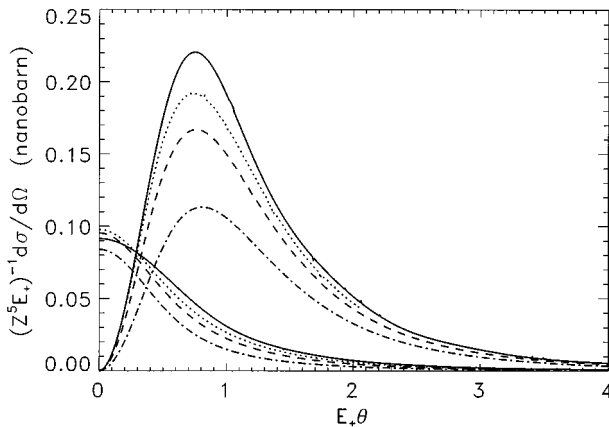

FIG. 9. Angular distribution of positrons at various energies for pair production with K-shell capture at targets with $Z=92$ (curves peaking at zero angle) and $Z=1$ (curves peaking for $E_+\theta$ near 1). The abscissa is the product of positron emission energy E_+ and angle θ, the ordinate is the differential cross section divided by E_+Z^5; units are mc^2 for E_+, radians for θ, and 10^{-33} cm^2 per steradian for the scaled differential cross section. The positron energies are $25mc^2$ (full curve), $15mc^2$ (dotted), $10mc^2$ (dashed), and $5mc^2$ (chained).
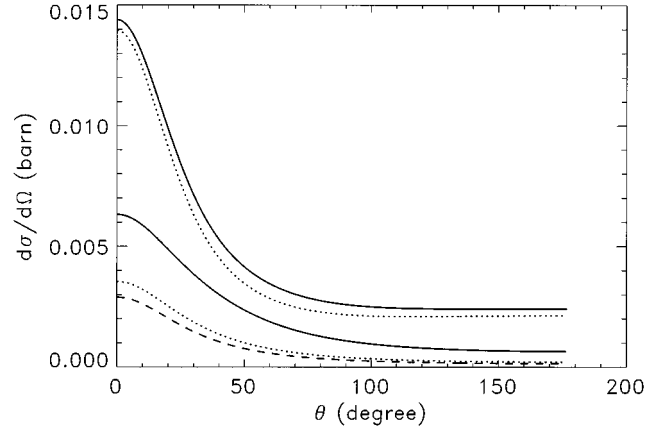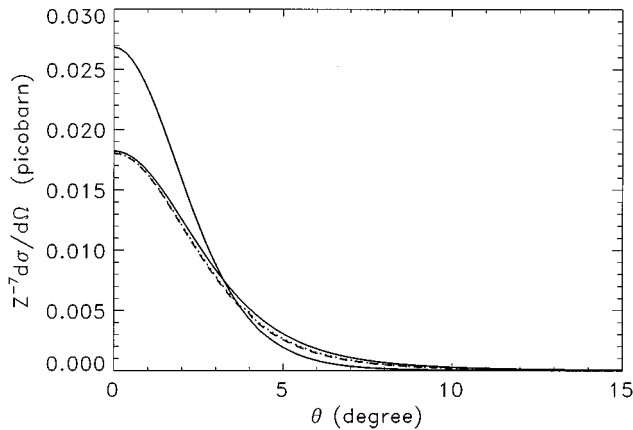
FIG. 11. Angular distribution of positrons at an energy of $10mc^2$ for pair production with capture to the $2p_{1/2}$ state. The differential cross section is divided by Z^7 and shown for nuclear charges of $Z=92$ (lower full-drawn curve), 82 (dotted), 79 (dashed), and 1 (upper full-drawn curve). The unit on the ordinate is 10^{-36} cm^2 per steradian.

B. Polarization effects

If the incoming photon is polarized so that it is assumed to have, say, circular polarization corresponding to positive helicity, the created positrons will be more or less polarized. The degree of polarization is measured by the polarization function defined as

$$P(\vartheta) = \frac{d\sigma(\sigma=1) - d\sigma(\sigma=-1)}{d\sigma(\sigma=1) + d\sigma(\sigma=-1)}. \qquad (63)$$

When $P=1$ (respectively, -1), the emitted positron is completely polarized in the direction of motion (respectively, in the direction opposite the direction of motion). Because of the angular-momentum selection rules, positrons emitted in the forward and backward directions are always completely polarized. Figure 12 displays the polarization function for a light and a heavy element. It may be noted, that for a hydrogen target, the polarization becomes complete for ϑ about 50

degrees for $E_+=1.5$, and for ϑ about 10 degrees for $E_+=10$. This is in agreement with the Born approximation according to which the polarization transfer is complete at an angle given approximately by [28]

$$k_0(k_0-1)(1-\beta\cos\vartheta) = 2. \qquad (64)$$

Indeed, this formula predicts that the complete polarization transfer should occur at $\vartheta=51.5$ degrees for $E_+=1.5$, and for $\vartheta=9.3$ degrees for $E_+=10$. This may be compared to our values of 52.0 and 9.3 degrees, respectively. Hence, we note that our predictions reproduce those of the Born approximation in the low-Z limit. The better agreement at the higher energy reflects the well-known fact that the accuracy of the Born approximation increases with energy. Furthermore, we note that the absence of complete polarization transfer at intermediate angles for high Z again demonstrates the complete breakdown of the Born approximation at high target charges.

As to the L shell, we mention that the polarization function for the $2p_{1/2}$ state is completely different from the s polarizations shown in Fig. 12 for all charge numbers. For $Z=1$ the complete polarization transfer observed at a definite intermediate angle for the K shell is replaced by a complete polarization reversal (complete spin flip). And, again, the result for high charge numbers is completely different from that pertaining to low values of Z.

IV. REMARKS ON HEAVY ION IMPACT

The photo cross sections obtained in Sec. II may be applied in a Weizsäcker-Williams construction to estimate the contribution to bound-free pair production in distant heavy-ion collisions. The relativistic projectile ion of atomic number Z_p is assumed to move on a rectilinear path at a constant velocity v throughout the collision and the electromagnetic field which it generates is ascribed to an equivalent bunch of photons which then interacts with the target nucleus through the previously determined photo cross sections, cf. [29], [30]. This leads to a cross section for ion impact of
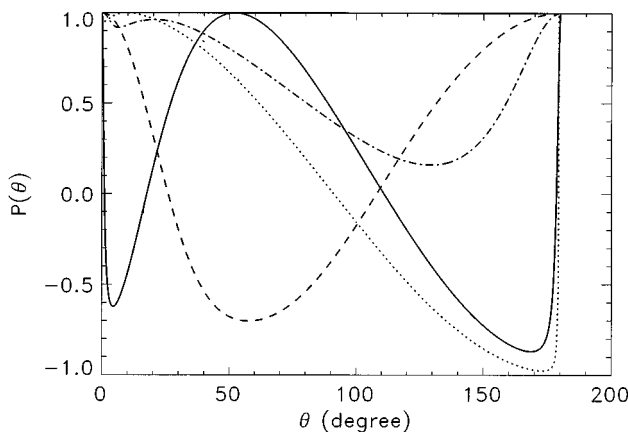

FIG. 12. Polarization. The full-drawn curve displays the polarization function (63) for production of K electrons for unit nuclear charge and positron emission at an energy E_+ of $1.5mc^2$, the dotted curve shows the same result for $Z=1$ and $E_+=10$, the dashed is for $Z=92$ and $E_+=1.5$, while the chained curve displays the polarization function for $Z=92$ and $E_+=10$.
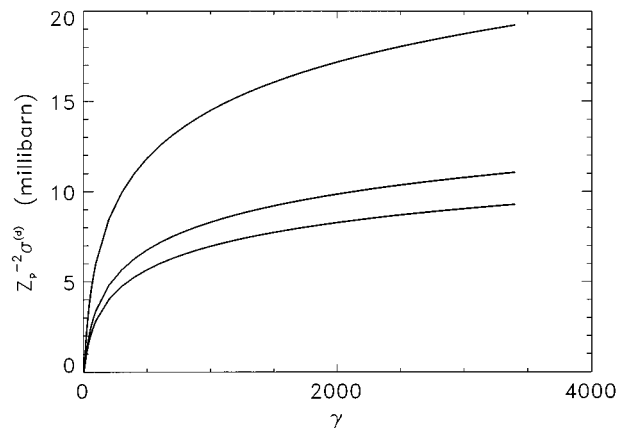
FIG. 13. Distant-collision contribution to the cross section for pair production with capture to the K shell for ion impact with γ values up to 3400. The cross section has been divided with the square of the projectile charge number and the ordinate is given in units of 10^{-27} cm^2. The lower curve corresponds to a target charge number of 79, the central curve to 82 while the upper curve corresponds to $Z=92$.

TABLE III. Distant-collision contribution to the cross section for pair production for bare gold ions incident on a bare uranium nucleus. The produced electron ends up in the K shell of the hydrogenlike uranium system. Cross sections are given in barn. The first column identifies the impact kinetic energy given in GeV/amu, the next two give our results for $b_{\min}=2$ and $b_{\min}=1$, the fourth column compares to the results of Aste *et al.* [4], and the last two compares to the Born approximation results of [32] and [33]. The Born results for the total cross section are taken from [32] for the two lower energies and estimated for the higher by scaling the result $\sigma_{\text{pert}}^{\text{total}}\simeq 14.3\ln\gamma-31$ given in [33] for impact of lead on lead with $Z_p^2 Z^5 f(Z)$, where $f(Z)$ is defined by Eq. (54) and listed in Table I. The Born results for $b\leqslant 2$ are estimated from [32] and [33] by numerical integration of data presented in a figure, respectively, by scaling a fitting formula with $Z_p^2 Z^5 f(Z)$.

Energy	Present; $b_{\min}=2$	Present; $b_{\min}=1$	Aste *et al.*; $b_{\min}=1$	$\sigma_{\text{pert}}^{b\leqslant 2}$	$\sigma_{\text{pert}}^{\text{total}}$
10	5.58	13.1	-	8	15
100	39.8	54.8	54.4	13	50
20.000	165	182	185	22	167

$$\sigma_{\text{ion}}^{(d)}=\int d\omega\ \sigma(\omega)\frac{dI^{(d)}(\omega)/d(\omega)}{\omega},\qquad(65)$$

where superscript (d) signifies distant collisions and $\sigma(\omega)$ is the cross section for photon impact. The photon intensity spectrum is given as [30]

$$\frac{dI^{(d)}}{d\omega}=\frac{2\alpha Z_p^2}{\pi v^2}\left[xK_0(x)K_1(x)-\frac{1}{2}v^2 x^2[K_1^2(x)-K_0^2(x)]\right],$$

$$x=\frac{\omega b_{\min}}{\gamma v},\qquad(66)$$

where K_0 and K_1 denote modified Bessel functions of the second kind and the quantity γ is the usual Lorentz factor $\gamma=1/\sqrt{1-v^2}$. The total spectrum (66) has been obtained by integrating the spectrum pertaining to a given impact parameter b over impact parameters beyond the minimum value $b_{\min}$. The latter quantity should be chosen such that beyond $b_{\min}$, the interaction between the projectile ion and the target system, defined here to be the ion which ends up dressed with an electron, is perturbative. Furthermore, the very concept of a well-defined impact parameter to the target system demands that b be in excess of the extension of the struck system. As for the case of inner-shell ionization, this implies that $b_{\min}$ cannot be smaller than the radius of the considered shell, cf. [29]. The contribution from close collisions has to be estimated by other means [31]. However, at high energies, the close-collision contribution is of minor importance, as the total cross section is dominated by the distant-collision contribution.

As an illustration, we consider charged particle impact on three different heavy ions corresponding to Z values of 79, 82, and 92. For production of K-shell electrons we choose as minimum impact parameter a length which essentially re-

flects the radius of the corresponding K shells, that is, neglecting minor variations between the three target ions, we choose $b_{\min}=2$. It should be noted, that this values is twice that chosen by most other authors who select the Compton wavelength for $b_{\min}$ irrespectively of the actual width of the electronical orbit. In Fig. 13 we show the distant-collision contribution to the pair production cross section as a function of the impact γ obtained by applying the K-shell photo cross sections derived in Sec. II in the formulas (65) and (66) above (for $\omega>50$ we actually applied the Born result (52) multiplied by the factor $f(Z)$).

In Table III we compare the results of the present work to those obtained in [4] also by the virtual photon method as well as to other calculations, as reported in [32] and [33], which are perturbative in the projectile field but based on exact Coulomb waves for the target states. The question of higher-order couplings to the projectile is not to be addressed here, see, e.g., [33] for an investigation based on a coupled channels approach or the two papers mentioned in [3] for an examination based on a direct numerical solution of the time-dependent one-electron Dirac equation. For the sake of the comparison, we include results obtained with our photo cross sections for $b_{\min}=1$. We note that with the latter choice, our results essentially reproduce those of [4] and that, by chance, the results obtained by the choice $b_{\min}=1$ essentially equal the sum of our results for $b_{\min}=2$ and an estimate of the contribution for close collisions. Furthermore, the Born result for the distant collisions, obtained by taking the difference between the last two columns in Table III, is close to our result for $b_{\min}=2$ at all three energies.

It may be noted, that in view of the shell ratios displayed in Fig. 7 ion-induced bound-free pair production is increased by roughly 20% beyond the values displayed in Fig. 13 and Table III when production of L electrons is included. Inclusion of all shells beyond the L shell probably contributes an additional 10%, see also the discussion at the end of Sec. II.

[1] See, for instance, the following reviews and references therein: C. A. Berturlani and G. Baur, Phys. Rep. **163**, 299 (1988); J. Eichler, *ibid.* **193**, 167 (1990); J. Eichler and W. E. Meyerhof, *Relativistic Atomic Collisions* (North-Holland, Amsterdam, 1995).

[2] See, for instance, Brookhaven National Laboratory, Formal

Report BNL 52195, 1989 (unpublished).

[3] See, for instance, K. Momberger, A. Belkacem, and A. H. Sørensen, Europhys. Lett. **32**, 401 (1995) and Phys. Rev. A **53**, 1605 (1996).

[4] A. Aste, K. Hencken, D. Trautmann, and G. Baur, Phys. Rev. A **50**, 3980 (1994).

[5] A more detailed write-up of the work presented is currently available on the World Wide Web on the address: http://www.dfi.aau.dk/~ahs/agger_thesis.ps

[6] H. A. Bethe and E. E. Salpeter, *Quantum Mechanics of One-and Two-Electron Atoms* (Springer, Berlin, 1957).

[7] E. Merzbacher, *Quantum Mechanics* (Wiley, New York, 1971).

[8] W. Greiner, *Relativistic Quantum Mechanics — Wave Equations* (Springer, Berlin, 1990).

[9] I. I. Sobel'man, *Atomic Spectra and Radiative Transitions*, 2nd ed. (Springer, Berlin, 1992).

[10] M. Weissbluth, *Atoms and Molecules* (Academic, San Diego, 1978).

[11] I. Øverbø, K. J. Mork, and H. Olsen, Phys. Rev. **175**, 443 (1968).

[12] W. R. Alling and W. R. Johnson, Phys. Rev. **139**, A1050 (1965).

[13] W. R. Johnson, D. J. Buss, and C. O. Carroll, Phys. Rev. **135**, A1232 (1964).

[14] One might look one more time on the integral in Eq. (39) and note that this integral is only convergent if $s + s_b - \iota < 0$. If not, it is divergent. As a matter of fact, this condition is not fulfilled for all the integrals appearing in the sum (36). The divergence is artificial and introduced by the expansion (35). This is also discussed by Øverbø, Arkiv for Det Fys. Seminar Trondheim **9** (1970), and by Alling and Johnson [12]. The solution is to multiply the integrand by a factor r^m, m being a real number chosen large enough for the integral to exist: after that, m is set equal to zero.

[15] As Sørensen and Belkacem, Phys. Rev. A **49**, 81 (1994), we might arrive at the very same result by using, not the integral representation for the confluent hypergeometric function, but the series expansion. This would lead to the same result, with the hypergeometric function expressed by the Gauss series. The present approach is more general, however, since it is immediately valid in the case $|2p/(p+k_0+ip_0)| > 1$, where the Gauss series fails to converge. This makes no difference at all for the calculations considered in the present work, but for calculations involving the photoelectric effect the Gauss series would be inapplicable. Indeed, the only reason for introducing the Kummer transformation in Eq. (44) was that this step gives the expressions a form that enables us to use the Gauss series.

[16] F. Sauter, Ann. Phys. (Leipzig) **11**, 454 (1931).

[17] R. H. Pratt, Phys. Rev. **117**, 1017 (1960).

[18] A. I. Milstein and V. M. Strakhovenko, Zh. Éksp. Teor. Fiz. **103**, 1584 (1993); [JETP **76**, 775 (1993)].

[19] The original formula published by Hall, Rev. Mod. Phys. **8**, 358 (1936), is not a good approximation — despite so stated by various authors including Heitler in the discussion of the photoelectric effect in his book, cf. [20].

[20] W. Heitler, *The Quantum Theory of Radiation* (Dover, New York, 1984).

[21] In order to obtain an early convergence with energy, our values of $f(Z)$ are actually determined as the high-energy limit of the ratio of the numerically determined cross section to Eq. (52) rather than to Eq. (53).

[22] R. H. Pratt, A. Ron, and H. K. Tseng, Rev. Mod. Phys. **45**, 273 (1973).

[23] R. H. Pratt, Phys. Rev. **119**, 1619 (1960).

[24] M. Gavrila, Phys. Rev. **124**, 1132 (1961).

[25] M. E. Rose, *Relativistic Electron Theory* (Wiley, New York, 1961).

[26] It may be noted that, for production of free pairs, the Born approximation gives a maximum in the forward direction, cf. Heitler [20]. For the related processes of the photoelectric effect and bremsstrahlung, a similar situation is encountered with the Born approximation yielding a zero in the forward direction for the former process but a maximum for the latter. This asymmetry of the Born results for the bound-free and free-free processes has caused some concern over the years. For instance, Fano, McVoy and Albers, Phys. Rev. **116**, 1147 (1959), tried to apply a detailed balance argument to show that the photoelectric effect must have the same angular distribution as bremsstrahlung if the final-state electron momentum is equivalent to that of the ground state, hence, they argued, the first Born approximation must be invalid. However, this argument does not hold: Gavrila's second-order Born approximation also vanishes in the forward direction, cf. [24] [note that the author erroneously states the contrary in Phys. Rev. **113**, 514 (1959)], and the present exact calculations also give results in good agreement with the Born approximation.

[27] W. R. Johnson, Phys. Rev. **159**, 61 (1967).

[28] H. Olsen, Springer Tracts Mod. Phys. **44**, 83 (1968).

[29] E. J. Williams, Kgl. Dan. Vidsk. Selsk. Mat. Fys. Medd. XIII, No. 4 (1935).

[30] J. D. Jackson, *Classical Electrodynamics* (Wiley, New York, 1975).

[31] In order to estimate the close-collision contribution, one could be tempted to apply the so-called sudden-collision approximation; for the latter see, e.g., K. Adler and Aa. Winther, Kgl. Dan. Vidsk. Selsk. Mat. Fys. Medd. XXXII, No. 8 (1960), and J. Eichler, Phys. Rev. A **15**, 1856 (1977). This implies an evaluation of matrix elements between initial and final states of the operator $\exp(i\chi)$, where χ is the time integral of the perturbing potential. However, it should be realized that two approximations are applied to reach this result. The calculation is performed in the interaction representation. First, in an expansion involving commutators of the interaction potential at different times, only the lowest-order nonvanishing term is retained. Second, in the remaining term the usual Schrödinger representation is used for the potential rather than the interaction representation. While the first approximation is valid due to the rapid variation of the electromagnetic field of the relativistic projectile, the second is highly questionable. Essentially, the second approximation corresponds to neglect of a phase factor which varies over distances of order $v/(E_b+E)$ and this length is certainly not large compared to the extent of the bound state.

[32] U. Becker, N. Grün, and W. Scheid, J. Phys. B **20**, 2075 (1987).

[33] A. J. Baltz, M. J. Rhoades-Brown, and J. Weneser, Phys. Rev. A **50**, 4842 (1994).